ARTICLE

Rational design, supramolecular synthesis and solid state characterization of two bicomponent solid forms of Mebendazole
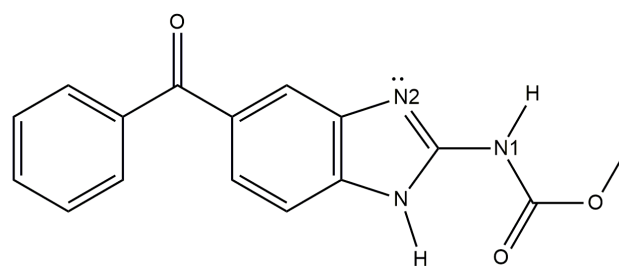
Eduardo L. Gutiérrez[1], Agustín A. Godoy[2], Griselda E. Narda[2] and Javier Ellena[3]*

Two novel bicomponent solid forms of mebendazole (MBZ), were developed as a mean to modulate its psychochemical and pharmaceutical properties. Supramolecular synthesis of MBZ A or C with perchloric or methylsulfuric acids, yields two salts of 1:1 stoichiometry which were analyzed through single crystal X-ray diffraction. MBZ perchlorate crystallizes in the $P2_1/n$ space group, while MBZ methylsulfate crystallizes in the $P-1$ space group. The API and its counter ions are interconnected in both crystal packings by a $R_2^2(8)$ supramolecular motif. 3-dimentional crystal structure is also stabilized by others strong intermolecular hydrogen bonds as well as non-classical interactions. FT-IR spectra are consistent with the inclusion of the anions in the crystal structure. MBZ perchlorate is stable up to 210 °C, when it undergoes the endothermic loss of the ester moiety. MBZ methylsulfate is stable up to 160 °C when occurs the endothermic elimination of the methylcarbamate moiety. The solubility behavior of MBZ perchlorate, studied by UV-visible spectroscopy, suggests an improvement by a factor of seven respects to MBZ A, in the apparent solubility of MBZ in 0.1 mol L^{-1} HCl. Further experiments are required to evaluate both the stability of the solids and the maximum solubility of the API.

Introduction

Mebendazole (MBZ, methyl N-(5-benzoylbenzimidazol-2-yl) carbamate, **Scheme 1**) is a broad-spectrum benzimidazole-derivate anthelmintic and postulated as a possible antitumor drug.[1] It is a Class II drug of the Biopharmaceutical Classification System[2] due to its poor solubility either in water or 0.1 mol L^{-1} HCl (aq) but high permeability[3] and it is included in the World Health Organization (WHO) Model List of Essential Drugs[4]. This active pharmaceutical ingredient (API) presents three polymorphs named as A, B and C that exhibit marked differences in their physicochemical properties and bioavailability.[5] MBZ A is the least water soluble form being MBZ B the most soluble one, while MBZ C presents an intermediate solubility value (9.84 ± 0.05, 71.3 ± 0.5 and 35.4 ± 0.5 mg L^{-1} respectively in pure water). This last one solid form is the therapeutically preferred one to treat several parasite infections (ascariasis, uncinariasis, oxyuriasis, and trichuriasis)[6-8]. Such is the importance of the polymorph choice that the International Pharmacopoeia 5th Edition restricts the suitable polymorphic form to MBZ C in chewing tablets, emphasizing that the overall manufacturing process

[1]INQUISAL–CONICET, San Luis, Argentina – Área de Química Física, Facultad de Química, Bioquímica y Farmacia, Universidad Nacional de San Luis. Chacabuco y Pedernera 5700, San Luis, Argentina.
[2]Instituto de Investigaciones en Tecnología Química (INTEQUI), Almte. Brown 1500-1402, D5700APA, San Luis – Área de Química General e Inorgánica "Dr. G. F. Puelles", Facultad de Química, Bioquímica y Farmacia, Universidad Nacional de San Luis, Chacabuco y Pedernera, 5700 San Luis, Argentina.
[3]Instituto de Física de São Carlos, Universidade de São Paulo, CP 369, 13.560-970, São Carlos, SP, Brazil.
* e-mail address: javiere@ifsc.usp.br
Electronic Supplementary Information (ESI) available: [details of any supplementary information available should be included here]. See DOI: 10.1039/x0xx00000x

should be designed and controlled to minimize its conversion into the more stable polymorph A.[8,9]

methyl N-(5-benzoyl-1H-benzimidazol-2-yl) carbamate
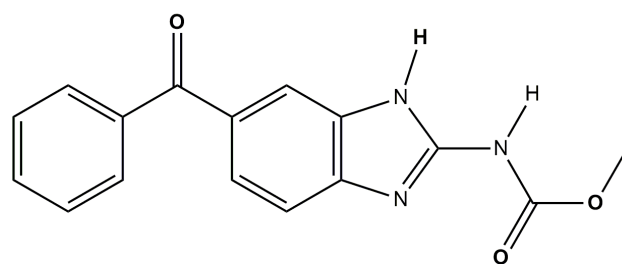
methyl N-(5-benzoyl-3H-benzimidazol-2-yl) carbamate

Scheme 1. *Above:* the 1H-tautomer of MBZ found in polymorph C. *Below:* The 3H-tautomer found in MBZ A.

MBZ presents enamine-imino tautomerism in solution.[10] As stated by Agatonovic-Kustrin *et al.*[8], tautomerism is responsible for MBZ polymorphism. The 1H-tautomer shown in **Scheme 1** *(above)* is the only one present in MBZ polymorph C, while MBZ polymorph A is formed by the crystallization of the 3H-tautomer shown in **Scheme 1** *(below)*. The crystal structure of polymorphs A and C have been previously

reported[11,12], while the structure of polymorph B remains undetermined. These three polymorphs show differences in their physicochemical and mechanical properties, which are related to numerous other pharmaceutical interesting properties (drug dissolution, absorption and bioavailability, but also manufacturing reproducibility, stability in storage and transport, etc.). De Villiers *et al.* have studied the thermal stability of MBZ polymorphs.[13] They characterized the first-order phase transition from polymorph C to A at approx. 200 °C and found evidence of a similar transformation from MBZ B into MBZ A. It have been recently reported that the MBZ most stable form A does not melt but rather decomposes above its thermal stability of approx. 200 °C.[14,15]

Regarding the relationship between the physicochemical properties and pharmaceutical performance, on one hand due to its high stability and therefore extremely low water solubility, therapeutic assays suggest that MBZ A has similar efficacy to placebos in controlling worm infections. On the other hand, the most soluble and least stable polymorph B has shown to be more toxic during both anthelmintic and anticancer tests.[16] MBZ C falls right into the therapeutic window, since its dissolution profile and its solubility ensure acceptable efficacy, meanwhile concentration values that can cause toxicity are not reached. However, polymorph interconversion has been demonstrated to occur in tablets prepared with form C, which suffer a transformation to products containing form A under the effects of moisture and heat. Due to the same phenomenon, suspensions of polymorph C may also contain part of their active principle converted to polymorph A.[17] This polymorph interconversion in solid drug formulations is a big problem for the pharmaceutical industry.

In this work, we developed two novel bicomponent solid forms of MBZ aiming to increase the knowledge about its intermolecular interactions as a mean to explore the possible ways to modulate properties such as solubility and thermal stability and to avoid polymorph interconversion. The design and synthesis of multicomponent systems using crystal-engineering techniques is a strategy widely used to improve the performance and processability of Active Pharmaceutical Ingredients (APIs). This approach has been also used to modulate the pharmacokinetic properties of the API solid form since it does not modify the intrinsic chemical structure of the drug but only its supramolecular environment.[18,19]

Here we use methylsulfuric (HSO_4CH_3) and perchloric ($HClO_4$) acids as coformers. HSO_4CH_3 is used as counterion in some drug formulations registered in the FDA Orange Book 40th Edition.[20] In contrast, there is not much literature about multicomponent drug crystals incorporating perchloric acid and.[21] Since sulfur and chlorine present similar size, $HClO_4$ was chosen as a HSO_4CH_3 analogue in an attempt to evaluate the effect in the crystal packing of the presence/absence of methyl group in the coformer. Both systems were designed based on the statistical probability of formation of a supramolecular heterosynthon of the $R_2^2(8)$ type[22] between the MBZ molecule and the appropriate coformers instead of the highly stable MBZ···MBZ homosynthon (**Tables S1** & **S2**, Electronic

Supplementary Information –ESI–). As shown in **Scheme 1** (*above*), MBZ 1H-tautomer exhibits one polarized ***N1−H*** bond that could act as hydrogen-bond (H-bond) donor, and one basic site on ***N2*** that could act as H-bond acceptor; this particular structure may allow the assembly of one MBZ molecule with a suitable coformer by two complementary intermolecular hydrogen bonds. Another similar $R_2^2(8)$ synthon could be designed for the 3H-tautomer (**Scheme 1**, *below*) involving ***N3*** as H-bond acceptor and ***N1−H*** as H-bond donor. In the **Tables S3** & **S4** we present the $R_2^2(8)$ synthons found among the cocrystals and salts reported in the literature[23–28], including one nitrate salt previously reported by us[29]. Concerning these specific chosen coformers, we also had to be aware of possible proton transfer, prior to crystallization, and therefore the salification of the API. Drug salts usually tend to convert to the raw APIs. Previous reports show that MBZ salts undergo a solvent-mediated transformation to pure MBZ polymorph C[29,30]. Here we focus mainly on the description of the crystal structure of these systems, the study of its thermal stability and the corresponding suspension stability of both new solid forms. Hirshfeld surface analysis was performed to complement the atom-by-atom analysis of intermolecular interactions and the relative stability of both compounds. The Hirshfeld surface emerged from an attempt to define the space occupied by a molecule as whole in a crystal for the purpose of partitioning the crystal electron density into molecular fragments. Since this surface is defined by the molecule and the proximity of its nearest neighbours, it encodes information about intermolecular interactions which can be readily identified using the tools provided by Hirshfeld surface analysis.[31,32]

Experimental

Reagents

Samples of MBZ (295.29 g mol^{−1}) polymorphs A and C were kindly provided by Laboratorio de Control de Calidad de Medicamentos, UNSL. Purity of these samples was checked using PXRD. Absolute methanol (CH_3OH, Sintorgan, analytical grade) was used, without any further purification, as solvent for the suspension and dissolution of the drug. Perchloric acid (70% w/w, 1.68 g mL^{−1} (20 °C), 100.46 g mol^{−1}) and sulfuric acid (H_2SO_4, 98% w/w, 1.84 g mL^{−1}, (20 °C), 98.08 g mol^{−1}) were obtained from Merck and Tetrahedron, respectively, and used without further purification too. Methylsulfuric acid (also known as methyl bisulfate due to its monoprotic nature, 112.10 g mol^{−1}) was synthesized by direct esterification of H_2SO_4 with CH_3OH[33,34]. The reaction was carried out by slowly mixing 1 mL H_2SO_4 98% w/w with 9 mL of absolute CH_3OH in an open vessel at room temperature (approx. 22-25 °C) (***Caution: very exothermic reaction***). Esterification was verified using UV-Vis spectroscopy.

Supramolecular synthesis

A sample of MBZ polymorphs A or C of approx. 25 mg (0.10 mmol) was suspended in 10 mL of absolute CH_3OH at room

temperature with constant magnetic stirring (500 rpm), 50 µL of acid solution ($HClO_4$: 0.60 mmol and HSO_4CH_3 0.10 mmol) were added to achieve complete dissolution of the solid. After 10 min stirring, the solution was filtered. Finally, the solution was brought to 5 °C to achieve slow evaporation of the solvent. After approx. seven days, the formation of small, prismatic crystals was observed. These crystals were separated by filtration and washed several times with *n*-hexane. Powder X-ray diffraction and FT-IR spectroscopy were used to check the purity and identity of the solids, which were then kept at room temperature for further characterizations.

As mentioned before, it is important to be aware about the possible salification of the API. The empirical "pK$_a$ Rule" states that salt should be expected when the difference in pK$_a$ between the conjugated acid of the base and the acid is greater that approx. 2-3 units. Considering the values of pK$_a$ of MBZ conjugated acid (HMBZ$^+$, 4,43[35]) and those of $HClO_4$ (−10) and HSO_4CH_3 (−2.6), a proton transfer prior to crystallization is very likely ($\Delta pK_{a,1}$ = 14.43 and $\Delta pK_{a,2}$ = 7.03) which need to be confirmed by SCXRD.

Powder X-ray diffraction

Powder X-ray diffraction (PXRD) analysis was performed on a Rigaku *Ultima IV* diffractometer (Rigaku Corporation) using Cu Kα radiation, in a step mode, between 3-50° in 2θ with a scanning rate of 0.6° min^{-1} (2 s per step) and a step of 0.02°. The powder diffraction patterns were collected and processed with «SmartLab Studio-II» software, associated with the diffractometer.

FT-IR Spectroscopy

Fourier transformed infrared spectrum were recorded on a Nicolet *Protègè 460* spectrophotometer (Nicolet Instrument Corporation) provided with a CsI beamsplitter, in the 4000-400 cm^{-1} range with 64 scans and spectral resolution of 4 cm^{-1}, using the KBr pellet technique. Measures were collected and processed with the software «Omnic», associated to the spectrometer. The spectra at controlled increasing temperatures were obtained by placing the pellet in a variable-temperature homemade cell in the 25 °C - 250 °C range within air atmosphere.

Single-crystal X-ray diffraction

Suitable-sized clear crystals were selected for the single crystal X-ray diffraction experiments. The data were collected at room temperature (293(2) K) on a Bruker APEX-II diffractometer with CCD detector system equipped with a Mo source (λ = 0.71073 Å). Data integration, cell determination and final parameters were obtained using the software Bruker SAINT[36] included in APEX2[37] software suite. The structures were solved by direct methods through the program SHELXLT[38] and the model obtained was refined by full matrix least squares on F2 using the program SHELXLT[38], included in Olex2[39] software. All the hydrogen atoms were placed in calculated positions and refined with fixed individual

displacement parameters [$U_{iso}(H)$ = 1.2 U_{eq} or 1.5 U_{eq}] according to the riding model. The crystallographic information files (CIFs) were deposited in the Cambridge Structural Data Base[40] under the codes CCDC 1995782 and 1995783. Copies of the data can be obtained, free of charge, via www.ccdc.cam.ac.uk. Geometrical calculation, molecular representations, pictures and tables were performed by and/or generated with the MERCURY 4.3.1[41], PLATON[42] and PARST softwares, these last two incorporated in the WINGX 2020.1 suite[43].

Hirshfeld surface analysis

Hirshfeld surface analysis was performed using the software CrystalExplorer17[44] using the CIFs as input files. Hirshfeld surfaces for MBZH·ClO_4 and MBZH·SO_4CH_3 were mapped with d_{norm} over the range −0.35 to 1.25. Shape index and curvedness surfaces were mapped over the ranges −1.0 to 1.0 and −4.0 and 0.4 respectively. 2D-fingerprints plots were obtained for de y di between 0.4 and 2.6.

Thermal analysis

Thermogravimetric analysis (TGA) and differential thermal analysis (DTA) measures were obtained simultaneously with a Shimadzu *DTG-60* instrument (Shimadzu Inc.), using platinum pan, flowing air at 20 mL min^{-1}, and a heating rate of 10 °C min^{-1} from room temperature (RT) to 600 °C. TGA and DTA curves were collected and processed with «TA60» software, associated to the analyser.

UV-visible spectroscopy, solubility and stabilities studies

UV-visible absorbance measures were carried out in an Agilent *8454* UV-vis spectrophotometer (Agilent Technologies), collected and processed with «8453 UV Visible Chem station Rev.A.10.01» software associated to the instrument.

Equilibrium solubility of MBZH·ClO_4 at room temperature was evaluated and compared against those of mebendazole polymorphs A and C in 0.1 mol L^{-1} hydrochloric acid solution, using the shake flask saturation method[45]. Saturated solutions of the three solids were prepared by stirring an excess amount of the solids into 4 mL of the dissolution medium for a period of 48 hs (20 °C and 200 rpm) in a *SI-300R* shaker (Lab Companion). After sedimentation, the solutions were filtered through a 0.45 mm filter (Exacta). The identity of the solid sediments was checked by PXRD. UV-Vis spectroscopy was employed to measure MBZ concentration in the saturated solutions, applying a direct calibration method, using the absorbance maxima as a parameter proportional to the concentration. Saturated solutions were diluted in the dissolution medium to ensure working on the spectrophotometer linear range of response.

Results and discussion

Crystalline habit, identity and purity

MBZH·ClO$_4$ crystallize as yellowish/brownish small prismatic crystals, while MBZH·SO$_4$CH$_3$ crystallizes as elongated prismatic colorless crystals in the shape of needles (**Figure S1**, ESI).

Preliminary evidence about the identity of presumably new solid products was provided by their vibrational spectra and their powder X-ray diffractions patterns. These measures were performed prior to the single-crystal X-ray diffraction experiments. Ayala *et al.*[46] have established that the position of the band corresponding to the carbamate carbonyl stretching mode could fingerprints the crystalline forms of MBZ. This band appears at 1730 cm^{-1}, 1715 cm^{-1} and 1697 cm^{-1} for polymorphs A, C and B, respectively14, and at 1759 cm^{-1} and 1757 cm^{-1} in the MBZH·ClO$_4$ and MBZH·SO$_4$CH$_3$ spectra, respectively. Further evidence of the inclusion of the anions in the crystal structure was given by the identification of other bands. The bands assigned to the v_3 and v_4 modes of the perchlorate anion appears at 1115 cm^{-1} and 625 cm^{-1}, and the bands of the same modes of methylsulfate anion were found at 1113 cm^{-1} and 614 cm^{-1}. The bands corresponding to stretching modes of the methyl group of the anion appears at 2850 cm^{-1} and 2815 cm^{-1}, while the stretching modes of the methyl group of the carbamate moiety of MBZ are at 2955 cm^{-1} and 2917 cm^{-1}. IR spectra are shown in **Figure S2**.

The same solid MBZH·ClO$_4$ form was obtained from both MBZ A and MBZ C polymorph, while the solid MBZH·SO$_4$CH$_3$ was obtained just from MBZ C (synthesis from MBZ A was not tested). We compared the powder X-ray diffractions patterns of both solids with those calculated for MBZ A and MBZ C, and the experimental one of MBZ B previously reported[24,47] (**Figure 1**). This comparison ruled out the formation of any of the three polymorphs after solvent evaporation as a sub-product, since none of their characteristic peaks were observed in the experimental patterns of MBZH·ClO$_4$ and MBZH·SO$_4$CH$_3$. With these evidences, we performed the SC-XRD experiments.
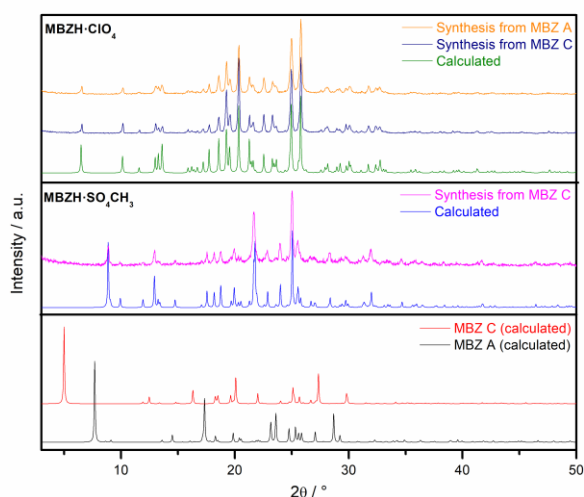

Figure 1. Experimental Powder X-ray diffractions patters of MBZ perchlorate and MBZ methyl sulfate compared with those calculated from solved structures.

PXRD pattern and FT-IR spectra analysis showed that both compounds, kept at room temperature, were stable in the solid state for at least for one year after the synthesis, and no evidence of the formation of any MBZ polymorph was found (**Figure S3**).

Structural description

Single-crystal X-ray diffraction experiments confirmed the formation of two new solids, mebendazole perchlorate (MBZH·ClO$_4$) and mebendazole methylsulfate (MBZH·SO$_4$CH$_3$). Both solids are ionic with a 1:1 stoichiometry.

Mebendazole perchlorate salt. This salt crystallizes in the monoclinic P2$_1$/n (14) space group. Crystal data, data collection and structure refinement parameters are shown in **Table 1**.

The crystal structure shows the total proton transfer from the perchloric acid to the **N2** of the imidazole ring of the drug, resulting in an ionic solid. An ORTEP type view of the asymmetric unit of MBZH·ClO$_4$, displaying the atoms labelling and the 50% probability ellipsoids, is shown in **Figure 2.A**.
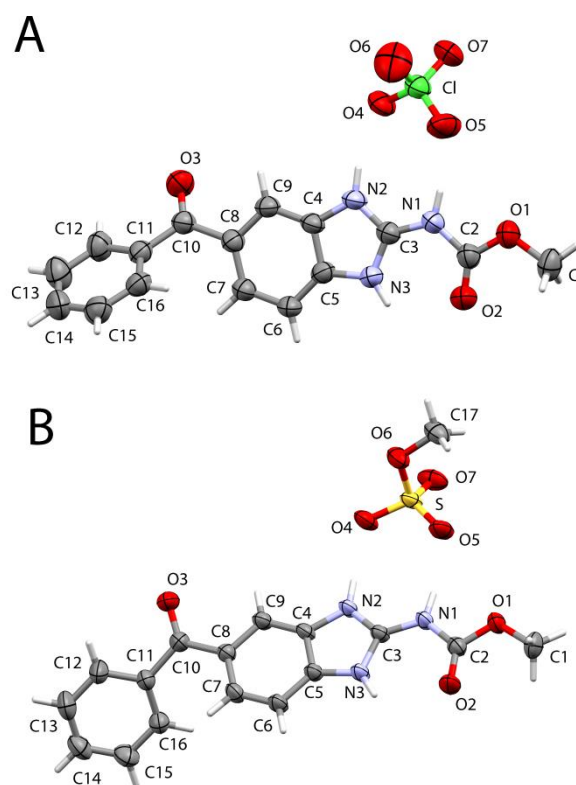

Figure 2. View of MBZ perchlorate (**A**) and MBZ methylsulfate (**B**) asymmetric units, showing the atoms labelling and the 50% probability ellipsoids for non-hydrogen atoms. The hydrogen atoms are shown as sticks of arbitrary radii. (Color code. C: grey; H: white; O: red; N: blue; Cl: green; S: yellow.)

Table 1. Crystal data, data collection and structure refinement parameters of MBZ perchlorate and MBZ methylsulfate.

Table 1

Identification code	MBZ perchlorate (MBZH·ClO₄)	MBZ methylsulfate (MBZH·SO₄CH₃)
Empirical formula	$C_{16}H_{14}ClN_3O_7$	$C_{17}H_{17}N_3O_7S$
Formula weight	395.75	407.39
Temperature / K	293(2)	293(2)
Crystal system	monoclinic	triclinic
Space group	P2₁/n (14)	P–1 (2)
a / Å	6.7934(7)	9.1092(11)
b / Å	9.2159(14)	9.9717(14)
c / Å	27.264(5)	9.9908(14)
α / °	90	92.075(12)
β / °	93.007(12)	102.401(11)
γ / °	90	90.209(10)
Volume / Å³	1704.5(4)	888.7(2)
Z/Z′	4	2
ρ_{calc} / g/cm³	1.542	1.528
μ / mm⁻¹	0.27	0.23
F(000)	816	424
Crystal size / mm³	0.25 × 0.18 × 0.15	0.16 × 0.05 × 0.02
Radiation	MoKα (λ = 0.71073)	MoKα (λ = 0.71073)
2Θ range for data collection / °	5.338 to 68.86	5.469 to 69.066
Index ranges	−10≤h≤9, −21≤k≤14, −40≤l≤34	−14≤h≤10, −15≤k≤14, −13≤l≤35
Reflections collected	10221	7683
Independent reflections	6430 [R_{int} = 0.066, R_{sigma} = 0.144]	64296 [R_{int} = 0.031, R_{sigma} = 0.115]
Data/restraints/parameters	6430/0/246	6296/0/255
Goodness-of-fit on F²	1.03	1.05
Final R indexes [I≥2σ(I)]	R_1 = 0.092, wR_2 = 0.204	R_1 = 0.065, wR_2 = 0.151
Final R indexes [all data]	R_1 = 0.244, wR_2 = 0.285	R_1 = 0.164, wR_2 = 0.188
Largest diff. peak/hole / e Å⁻³	0.54/−0.34	0.29/−0.35

Table 2. Hydrogen-bonding geometry for MBZ perchlorate and MBZ methylsulfate

Table 2

MBZ perchlorate				
D–H···A	**D–H** / Å	**H···A** / Å	**D···A** / Å	**D–H···A** angle / °
N3–H···O2	0.86	2.19	2.698(5)	117
N2–H···O4	0.86	1.94	2.787(5)	167
N1–H···O5	0.86	2.04	2.875(5)	162
N3–H···O7 [a]	0.86	2.14	2.919(5)	151
C7–H···O6 [b]	0.93	2.58	3.388(7)	146
MBZ methylsulfate				
D–H···A	**D–H** / Å	**H···A** / Å	**D···A** / Å	**D–H···A** angle / °
N3–H···O2	0.86	2.21	2.710(3)	117
N2–H···O4	0.86	1.89	2.742(3)	170
N1–H···O5	0.86	1.90	2.736(3)	163
N3–H···O7 [c]	0.86	2.04	2.800(3)	147
C7–H···O6 [d]	0.93	2.55	3.314(3)	140
C17–H···O2 [e]	0.93	2.53	3.422(4)	154

D: donor. A: acceptor
Equivalent positions:
a: x, y+1, z   b: x+1, y+1, z   c: x–1, y, z
d: −x+1, −y+1, −z+1   e: x+1, y, z

Protonation causes changes in the bond lengths of the imidazole ring. In the crystal structure of polymorph C[12], the length of the amine (**N3–C3**) and imine (**N2–C3**) bonds are significantly different: 1.349(9) Å and 1.30(1) Å, respectively.

On the other hand, in the MBZH⁺ cation, the bond **N2–C3** is 1.337(6) Å and the bond **N3–C3** is 1.321(6) Å, showing a partial loss of the double bond character due to the presence of a positive charge on **N2**. This behavior is caused by the displacement of the negative charge on the ring as a

consequence of protonation. It is also worth noting that protonation shortens the length of the bond **N1–C3**, due to an additional displacement of electron density from **N1** towards the site of protonation. This bond is 1.37(1) Å in MBZ C, while it is 1.341(6) Å in MBZH$^+$, suggesting a higher double bond character (**Figure S4**). These observations are consistent with the behavior exhibits by protonated MBZ molecule in all reported structures.

In the MBZH·ClO$_4$ crystal structure the MBZH$^+$ cation shows a methylcarbamate group coplanar with the benzimidazole ring, forming an intramolecular resonance-assisted H-bond (RAHB)[48] between the carbonylic oxygen **O2** (acceptor, A) and the imidazolic nitrogen **N3** (donor, D; **A···H**: 2.19 Å, **Table 2**). The MBZH$^+$ cation also shows a dihedral angle of 51.6(2)° between the least squares planes determined by the benzimidazolic and benzoyl rings (**Figure 3.D**).

The asymmetric unit of the solid consists of one MBZH$^+$ cation and one ClO$_4^-$ anion. Both ions form a supramolecular motif of the R$_2^2$(8) type stabilized by two intermolecular H-bonds: **N1–H···O5** (**A···H**: 2.04 Å) and **N2–H···O4** (**A···H**: 1.94 Å) (**Figure 3.B**). In **Table S3** we collected the H-bond distances of all MBZ salts that presents this supramolecular motif (no cocrystals were found exhibiting this synthon). This arrangement is not coplanar: there is a dihedral angle of 23.0(3)° between the planes determined by the atoms **N3**, **C3** and **N1**, and the atoms **O4**, **Cl** and **O5** of the perchlorate anion.
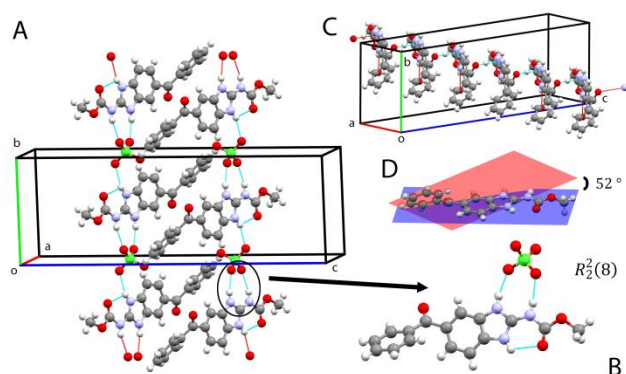

Figure 3.A. Antiparallel chains along b axis of ionic pairs MBZH$^+$/ClO$_4^-$ assembled by intermolecular H-bonds.
B. Supramolecular motif R$_2^2$(8) formed by one MBZH$^+$ cation and one ClO$_4^-$ anion. **C.** Arrangements of MBZH$^+$ in the plane ac stabilized by a peculiar benzoyl/imizadole interaction. **D.** Conformation of MBZH$^+$ cation in the crystalline state. (Color code. C: grey; H: white; O: red; N: blue; Cl: green.)

The ionic pairs MBZH$^+$/ClO$_4^-$ are connected along the **b** axis through H-bond interactions between the atom **N3** of one pair and the atom **O7** of the next pair (**A···H**: 2.14 Å). These chains are ordered in an antiparallel way with the ionic MBZH$^+$/ClO$_4^-$ pairs of opposite chains related by an inversion centers (**Figure 3.A**). In the **ac** plane, there is a short contact that contributes to crystal packaging, which was not found in others solid forms of the drug: the imidazolic **N2** connects with the bezoylic **O3** of

an adjacent molecule (3.012(5) Å). This interaction, also revealed by Hirshfeld surface analysis (see below), gives rise to the arrangement of MBZH$^+$ shown in **Figure 3.C**. Numerous other short-contact interactions can be found, which contribute to final stabilization of the crystal packing; among them, the **C3···O3** (2.951(6) Å) contact that reinforces the **N2···O3** interaction. The oxygen atoms of the perchlorate anions, where lies the negative charge of the compound, are involved in various short-range interactions. For instance, the atoms **O5** and **O7** interact with the atoms **C2** and **C1** of the methylester group at the end of a contiguous MBZ molecule in the **ac** plane

Mebendazole methylsulfate salt. Mebendazole methylsulfate crystallizes in the triclinic P–1 (2) space group. Crystal data, data collection and structure refinement parameters are listed in **Table 1**. An ORTEP type view of the asymmetric unit of MBZH·SO$_4$CH$_3$, displaying the atoms labelling and the 50% probability ellipsoids, is shown in **Figure 2.B**.

Protonation on **N2** produces here the same effects on the bond lengths of the imidazole ring as described in the previous section. Imine and amine bonds are very similar: the bond between **N2–C3** is 1.326(4) Å, and the bond **N3–C3** is 1.338(3) Å. The displacement of the electron density also shortens the length of the bond linking imidazole ring to the carbamate moiety (**N1–C3**: 1.341(3) Å) (**Figure S4**). In this salt, the MBZH$^+$ cation is found in a molecular conformation similar to the one adopted in the MBZH·ClO$_4$ crystal structure. The benzimidazole ring is coplanar with the carbamate moiety, and the resonance-assisted intramolecular H-bond between the imidazolic **N3** and carbonylic **O2** (**A···H**: 2.21 Å, **Table 2**) is also present. The dihedral angle determined by the least-square planes through the benzimidazolic and the benzoyl rings is 54.32(14)°.

The crystal packing of the MBZH·SO$_4$CH$_3$ also shows the presence of infinite chains connected by the same intermolecular synthon with R$_2^2$(8) motif, but in this case along the crystallographic **a** axis. These chains are stabilized by two intermolecular H-bonds: **N1–H···O5** (**A···H**: 1.90 Å) and **N2–H···O4** (1.89 Å) (**Figure 4.C**). This arrangement is almost planar: there is a dihedral angle of just 7.12(10)° between the least-squares planes through the **N3**, **C3** and **N1**, and **O4**, **S** and **O5** atoms. Each MBZH$^+$/SO$_4$CH$_3^-$ pair is connected to the next ionic pair through two intermolecular H-bond: **N3–H···O7** (2.04 Å) and **C17–H···O2** (2.53 Å). These interactions form antiparallel chains in the [100] direction. Ionic pairs of adjacent chains are related again by an inversion center, giving rise to the formation of dimers.

In **bc** plane, antiparallel chains are connected by a short contact between **O7** and **N1** (2.988(3) Å) (**Figure 4.A**). This inter-chains contact connect the chains in a A···B C···D sequence, since all polarized groups are exposed between chains "A" and "B", and "C" and "D", awith methyl groups from methylsulfate anions laying between chains "B" and "C". Two

non-classical H-bonds are found between chains "*B*" and "*C*" in which one methylsulfate from chain "*C*" acts both as acceptor (**O6**···**H–C7**, 2.55 Å) and donor (**C17–H**···**O3**, 2.68 Å) (**Figure 4.B**).

Adjacent chains are connected by two different contacts: one non-classical H-bond between **O5** and **C13** (A···H: 2.68 Å), and one interaction between the bezoyilic **O3** of one MBZH$^+$ and **C1** of next cation (3.213(4) Å), forming infinite layers parallel to **a** axis (**Figure S5**).
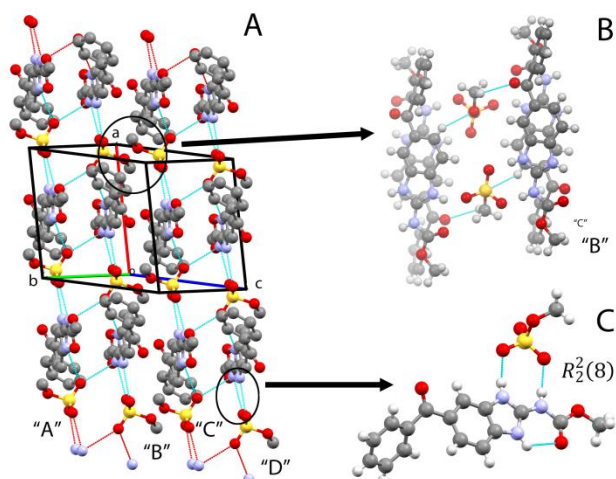
Figure 4.A. Antiparallel chains along **a** axis of ionic pairs MBZH$^+$/SO$_4$CH$_3^-$ assembled by intermolecular H-bonds.
B. Short-contact interactions *C–H*···*O* between "*B*" and "*C*" chains.
C. Supramolecular motif $R_2^2(8)$ formed by one MBZH$^+$ cation and one SO$_4$CH$_3^-$ anion. (Color code. C: grey; H: white; O: red; N: blue; S: yellow.)

Hirshfeld surface analysis. Hirshfeld surface analysis shows that, as expected, the predominant intermolecular interactions are the *N–H*···*O* H-bonds described in the previous sections, with the three *N* atoms of MBZH$^+$ acting as donors. These short H-bonds are associated with two large red spots on the d_{norm} [from -0.35 (blue) to 1.25 Å (red)] mapped on the Hirshfeld surface of the cation (**Figures 5A** & **B**).

However, the observation of the d_{norm} surface of MBZH$^+$ reveals that the **N3–H**···**O7** interaction is reinforced by an additional non-classical interaction **C6–H**···**O4** (A···H: 2.68 Å in MBZH·ClO$_4$ and 2.62 Å in MBZH·SO$_4$CH$_3$) (**Figures 5C** & **D**). Furthermore, there is another non-classical interaction **C17–H**···**O2** (2.53 Å) in MBZH·SO$_4$CH$_3$ in which the MBZH$^+$ cation acts as acceptor through the carbamic *O*. These longer contacts (and therefore weaker) are shown as faint red spots visible on the d_{norm} surface (**Figures 5D**).

The intermolecular contact **N2**···**O3** (3.012(5) Å) found in MBZH·ClO$_4$ is reinforced by another short contact interaction between **O3** and **C3** (2.951(6) Å) (**Figure S6A**). Both interactions are associated with a large red spot around **O3** on the d_{norm} surface. 2D-fingerprint plot reveals that this red spot presents an important contribution from this **C**···**O** contact (**Figure S6B**). The assembling of MBZH$^+$ cations in the **ac** plane

is also stabilized by carbonyl···π interactions between the benzimidazole moiety of one MBZH$^+$ and the carbamate moiety of the next molecule, revealed by the pattern of red and blue triangles on the shape index surface (**Figure S7A**). Curvedness surface plots show flat patches above one side of the benzimidazole ring, and on the opposite side above the carbamate moiety, suggesting the same pattern of planar stacking of MBZH$^+$ molecules (**Figure S7B**). These interactions are absent in MBZH·SO$_4$CH$_3$ and the arrangement of infinite layers is only stabilized by discrete short-contact interactions.
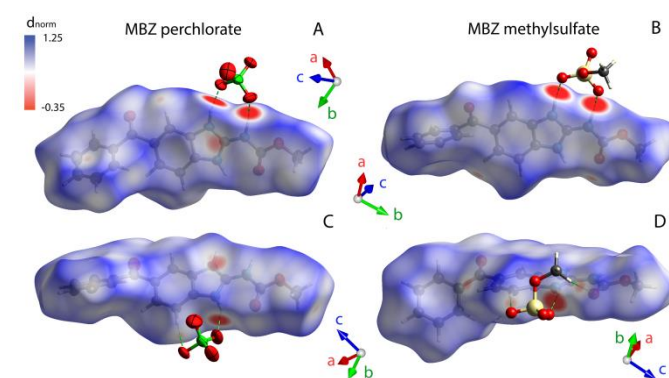

Figure 5. MBZH$^+$ cations in MBZH·ClO$_4$ (**A** & **C**) and MBZH·SO$_4$CH$_3$ (**B** & **D**) mapped with d_{norm} surface.

Thermal stability

Thermal analysis revealed MBZH·ClO$_4$ is stable up to 210 °C. DTA and DSC curves show a first endothermic event (Temp. onset 210 °C, Temp. centered at 239 °C) associated with a relative mass loss of 14.77%, as demonstrated by the TGA experiment, which is consistent with the mechanism proposed by Holanda *et al.* for MBZ degradation in air to form 2-amino-5-benzoylbenzimidazole[14]. The loss of the methylester moiety in MBZH$^+$ cation implies a theoretical mass loss of 14.66%. In order to obtain more evidence of this process, we conducted a temperature-variable FT-IR experiment. The progressive reduction of the intensity of the carbamate carbonyl band at 1759 cm^{-1} until it completely disappears, suggests that the same mechanism proposed by Holanda *et al.* operates in the first stage of MBZH·ClO$_4$ degradation.

Thermal analysis curves and temperature-dependent vibrational spectra are shown in **Figure 6** and **Inset**. This experiment shows an improvement in the drug thermal stability. In this way, this salt is even more stable than those salts and cocrystals previously reported (i.e.: MBZ mesylate monohydrate: 50 °C[25], MBZ nitrate: 150 °C, MBZ hydrochloride: 160 °C[44] and MBZ/valeric acid cocrystal: 186 °C). This stability could be attributed to the ability of the perchlorate anion to form a more stable supramolecular motif with the MBZ molecule, preventing the cleavage of the bond between the benzimidazole ring and the carbamate moiety at lower temperatures.
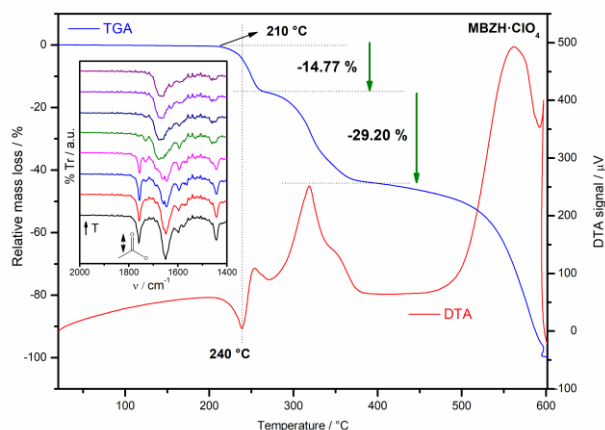
Figure 6. TGA and DTA curves of MBZ perchlorate. *Inset:* Temperature-variable FT-IR spectra of MBZ perchlorate.

A second stage of the thermal decomposition starts almost immediately (260 °C) and seems to involve two overlapped exothermic events with a relative mass loss of 29.00%. **Scheme S1** shows the propose decomposition mechanism in which the cleavage of the amine bond with the removal of ammonia is followed by the subsequent elimination of perchloric acid. Theoretical mass loss for these consecutives eliminations is 29.18%, in good agreement with the experimental value. The final stage is the complete degradation of the remaining compound, 5-benzoylbenzimidazole.

MBZH·SO$_4$CH$_3$ is stable up to 160 °C, when begins a relative mass loss of 19.77% (corrected: 17.98%) associated with an endothermic signal in the DTA curve (centered at 180 °C) consistent with the cleavage of the amine bond and the elimination of the entire methylcarbamate moiety (theoretical mass loss: 17.94%). Since the end of this event in TGA and DTA was not clear, we made use of the first derivate to identify it. The removal of methylsulfuric acid and the final degradation of the organic product seem to be overlapped and there is no defined temperature when these processes begin. Thermal analysis curves are shown in **Figures S9**. The laminar disposition of the ions in the crystal structure may be the cause of this lesser stability. The presence of the methyl groups of methylsulfate anions pointing towards the interior of chains "*B*" and "*C*" keep layers apart and reduce the ability of the anions to interact with the MBZ molecules, preventing a better stabilization of the crystal structure and reducing the thermal stability of the compound.

Differences in stability could also be understood in terms of the different patterns of intermolecular interactions revealed by Hirshfeld surface analysis. In both salts, $N–H\cdots O$ H-bonds are predominant; however these interactions represent a greater percentage of the d_{norm} surface in MBZH·ClO$_4$. Also, an important percentage of MBZH·SO$_4$CH$_3$ d_{norm} surface is associated with $H\cdots H$ contacts. In addition to that, the planar stacking arrangement of MBZH$^+$ in MBZH·ClO$_4$ is stabilized by two short contact interactions (with d_{norm} shorter than the sum of the van der Waals radii) and others $C\cdots C$ ($\pi\cdots C$) interactions,

while in MBZH·SO$_4$CH$_3$ the infinite layers are only stabilized by discrete short contacts, with d_{norm} greater than the sum of the van der Waals radii. **Scheme S1** shows the propose decomposition mechanisms for both salts.

MBZH·ClO$_4$ appears to be the most stable solid form of the API reported to date, while the stability of MBZH·SO$_4$CH$_3$ is similar to that of MBZ/butyric acid cocrystal (163.5 °C) previously reported by Chen *et al.* (2013)[28].

Solubility and stability in solution and in water suspension

Using the shake flask saturation method (USP) we determine an improvement in a factor of 7 in the apparent equilibrium solubility of MBZH·ClO$_4$ respect to MBZ A, in 0.1 mol L^{-1} hydrochloric acid solution. However, this experiment is not suitable for the determination of the equilibrium solubility of the API. This method is based on the assumption that the solid product does not undergo phase transitions or any other transformation during the experiment. This apparent solubility increase could be considered a drawback since it is similar to that of MBZ B which is toxic. Nevertheless, this increment is lesser than those previously reported for some MBZ salts and cocrystals also obtained by crystal engineering techniques[27].

MBZ salts reported here are metastable forms of the drug in the conditions of the equilibrium solubility experiment, and the transformation to a more stable phase occurs. After 48 hours in contact with the solvent, samples of MBZH·ClO$_4$ salt suffered a transformation process. As shown in **Figure S10**, the comparison of powder X-ray diffraction patterns of those samples, before and after the experiment, with those of MBZ polymorphs, shows that MBZH·ClO$_4$ transforms into MBZ A while previous reports indicate that other MBZ salts transforms into MBZ C in similar conditions[29,30]. This transformation can be justified by the great difference in solubility of the two components of the salt: the perchlorate anions completely dissolve in the solution, while the MBZ molecules precipitate to form the polymorph A. In order to determine a more representative value of the solubility of these salts, we designed a modified method that takes into account the kinetics of the process, both in the solution and in the solid phase, which we will apply to study the dissolution behaviour of several MBZ salts[30].

Once dissolved, MBZ exhibits a behaviour that is independent of its solid form. MBZ methanolic solution shows three bands in the UV region: 212 nm, 247 nm and 311 nm. In ultrapure water (pH 7), these bands are at 209 nm, 249, and 313 nm. The little effect of the solvent polarity on the position of these bands suggests an important hydrophobicity and poor solvation in polar media. The spectrum of MBZ shows a hypsochromic effect in 0.1 mol L^{-1} hydrochloric acid solution. The bands shift to lower wavelength (201, 233, and 287 nm) since the absorbent species in this medium is the cation MBZH+ (MBZ is completely protonated at pH $\cong$ 1). The anion MBZ(–H)$^-$ prevails at pH ≥ 10[35], and the excess of negative charge on the benzimidazole ring shifts the spectrum towards higher wavelengths (**Figure 7.A**).

Regarding its stability in solution, MBZ is extremely stable in methanol and in 0.1 mol L^{-1} hydrochloric acid solutions. The

spectra of MBZ solutions fresh and after several days of prepared (kept at 25 °C) show little changes in the intensities of the bands, attributed to the precipitation of the drug (**Figure 7.B**). On the other hand, MBZ undergoes a fast degradation process in water solutions when the pH of the medium is increased (**Figures 7.C** and **7.D**). This is in good agreement with the hydrolysis of carbamates extensively reported[49,50].
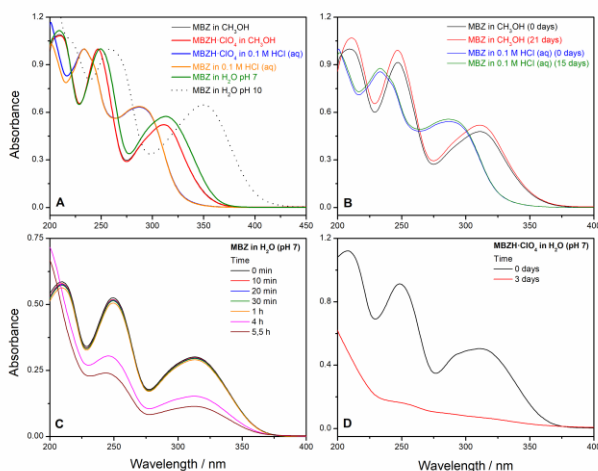

Figure 7.A. Mebendazole UV-visible spectra in water and methanol. **B.** Stability of mebendazole in methanol and 0.1 mol L^{-1} hydrochloric acid aqueous solution. **C.** Degradation of MBZ in water pH 7. **D.** Degradation of MBZH·ClO4 in water pH 7.

Conclusions

Two novel mebendazole (MBZ) bicomponent systems were developed and characterized in solid state and in solution. Recrystallization of MBZ with perchloric and methylsulfuric acids by slow solvent evaporation yielded two ionic solids forms of 1:1 stoichiometry: MBZ perchlorate (P2$_1$/n) and MBZ methylsulfate (P–1). As expected, both anions form a supramolecular motif of the R$_2^2$(8) type through the formation of two intermolecular $N–H\cdots O$ H-bonds. Ionic pairs are found in dimers related by an inversion center assembled in antiparallel chains by intermolecular H-bonds, acting the anions as bridges between MBZ molecules. Several other important H-bonds and short-contact interactions stabilized the crystal packings. Hirshfeld surface analysis revealed that the predominant intermolecular interactions are the $N–H\cdots O$ H-bonds where the three N atoms of MBZH$^+$ acts as donors. MBZ perchlorate is stable up to 210 °C, when occurs the endothermic elimination of the methylester moiety of the drug. We found an improvement in the thermal stability of the drug, since this salt is more stable than MBZ polymorph and other multicomponent systems previously reported. On the other hand, MBZ methylsulfate first degradation step begins at 160 °C and follows a different mechanism. These formulations avoided polymorph conversion and showed good stability in the solid state when they were stored at room temperature. Preliminary experiments showed an improvement in MBZ perchlorate with respect to MBZ in a factor of 7. However further experiments are needed to study the kinetics aspects

of both the dissolution process of these salts and the stability of the drug in aqueous media.

Conflicts of interest

There are no conflicts to declare.

Acknowledgements

Notes and references

1   P. Nygren, M. Fryknäs, B. Ågerup and R. Larsson, *J. Cancer Res. Clin. Oncol.*, 2013, **139**, 2133–2140.
2   H. V. Chavda, C. N. Patel and I. S. Anand, *Sys Rev Pharm*, 2010, **1**, 62–69.
3   J. Costa, M. Fresno, L. Guzmán, A. Igual, J. Oliva, P. Vidal, A. Pérez and M. Pujol, *Circ. Farm. - Barcelona*, 1991, **49**, 415–424.
4   World Health Organization, WHO 19th Model List of Essential Medicines (April 2015) (Amended November 2015), http://www.who.int/medicines/publications/essentialmedicines/en/
5   A. C. Evans, J. E. Fincham, M. A. Dhansay and W. Liebenberg, *South African Med. J.*, 1999, **89**, 1118.
6   E. Swanepoel, W. Liebenberg, B. Devarakonda and M. M. De Villiers, *Pharmazie*, 2003, **58**, 117–121.
7   E. Swanepoel, W. Liebenberg and M. M. De Villiers, *Eur. J. Pharm. Biopharm.*, 2003, **55**, 345–349.
8   S. Agatonovic-Kustrin, B. D. Glass, M. Mangan and J. Smithson, *Int. J. Pharm.*, 2008, **361**, 245–250.
9   W. Liebenberg, T. G. Dekker, A. P. Lötter and M. M. de Villiers, *Drug Dev. Ind. Pharm.*, 1998, **24**, 485–488.
10 Y. Kasetti and P. V. Bharatam, *Theor. Chem. Acc.*, 2012, **131**, 1–12.
11 F. F. Ferreira, S. Antonio Gutierrez, P. C. Pires Rosa and C. de O. Paiva-Santos, *Int. J. Drug Dev. Res.*, 2011, **3**, 26–33.
12 F. T. Martins, P. P. Neves, J. Ellena, G. E. Camí, E. V. Brusau and G. E. Narda, *J. Pharm. Sci.*, 2009, **98**, 2336–2344.
13 M. M. De Villiers, R. J. Terblanche, W. Liebenberg, E. Swanepoel, T. G. Dekker and M. Song, *J. Pharm. Biomed. Anal.*, 2005, **38**, 435–441.
14 B. B. C. Holanda, R. T. Alarcon, R. B. Guerra, D. Rinaldo, F. C. R. Spazzini, R. A. E. Castro and G. Bannach, *J. Anal. Appl. Pyrolysis*, 2018, **135**, 76–84.
15 R. L. Roque-Flores, J. F. de Oliveira, F. M. de S. Carvalho and J. do R. Matos, *J. Pharm. Innov.*, 2020, **15**, 116–124.
16 P. Charoenlarp, J. Waikagul, C. Muennoo, S. Srinophakun and D. Kitayaporn, *Southeast Asian J. Trop. Med. Public Health*, 1993, **24**, 712–716.
17 N. L. Calvo, T. S. Kaufman and R. M. Maggio, *J. Pharm. Biomed. Anal.*, 2016, **122**, 157–165.
18 D. J. Berry and J. W. Steed, *Adv. Drug Deliv. Rev.*, 2017, **117**, 3–24.

19 J. Wounters and L. Quéré, *Phamaceutical Salts and Co-crystals*, RSC Publishing, Cambridge, 2012.

20 Food and Drug Administration (FDA), U.S. Department of Health and Human Services, Approved Drug Product with Therapeutic Equivalence Evaluations 40th Edition ("Orange Book") (2020), http://www.fda.gov/drugs/drug-approvals-and-databases/approved-drug-products-therapeutic-equivalence-evaluations-orange-book

21 Y. Ma, S. Ge, W. Wang, Q. Zheng, Y. Zuo, C. Zhong and B. Sun, *J. Mol. Struct.*, 2016, **1105**, 1–10.

22 P. Deepa, R. Vijay Solomon, S. Angeline Vedha, P. Kolandaivel and P. Venuvanalingam, *Mol. Phys.*, 2014, **112**, 3195–3205.

23 N. M. Blaton, O. M. Peeters and C. Deranter, *Cryst. Struct. Commun.*, 1980, **9(1)**, 181–186.

24 E. V. Brusau, G. E. Camí, G. E. Narda, S. Cuffini, A. P. Ayala and J. Ellena, *J. Pharm. Sci.*, 2008, **97**, 542–552.

25 K. de Paula, G. E. Camí, E. V. Brusau, G. E. Narda and J. Ellena, *J. Pharm. Sci.*, 2013, **102**, 3528–3538.

26 M. Caira, T. Dekker and W. Liebenberg, *J. Chem. Crystallogr.*, 1998, **28**, 11-15.

27 J.-M. Chen, Z.-Z. Wang, C.-B. Wu, S. Li and T.-B. Lu, *CrystEngComm*, 2012, **14**, 635-640.

28 J. Chen and T. Lu, *Chinese J. Chem.*, 2013, **31**, 635–640.

29 E. L. Gutiérrez, M. S. Souza, L. F. Diniz and J. Ellena, *J. Mol. Struct.*, 2018, **1161**, 113–121.

30 G. E. Camí, E. V. Brusaua, G. E. Narda and R. M. Maggio, *J. Drug Deliv. Sci. Technol.*, 2020, **15**, 101344.

31 J. J. McKinnon, M. A. Spackman and A. S. Mitchell, *Acta Crystallogr. Sect. B*, 2004, **B60**, 627–668.

32 M. A. Spackman and D. Jayatilaka, *CrystEngComm*, 2009, **11**, 19-32.

33 E. C. Minerath, M. T. Casale and M. J. Elrod, *Environ. Sci. Technol.*, 2008, **42**, 4410–4415.

34 C. P. Mumma and R. O. Hoiberg, *J. Am. Chem. Soc.*, 1969, **91**, 4273–4278.

35 H. Wan, A. G. Holmén, Y. Wang, W. Lindberg, M. Englund, M. B. Någård and R. A. Thompson, *Rapid Commun. Mass Spectrom.*, 2003, **17**, 2639–2648.

36 SAINT, Version 7.60a, Bruker AXS Inc, Madison, WI, USA, 2006.

37 Bruker AXS I. APEX2 Version 2.1-0, 2004.

38 G. M. Sheldrick, *Acta Crystallogr. Sect. A*, 2015, **A71**, 3–8.

39 O. V. Dolomanov, L. J. Bourhis, R. J. Gildea, J. A. K. Howard and H. Puschmann, *J. Appl. Crystallogr.*, 2009, **42**, 339–341.

40 F. H. Allen, *Acta Crystallogr. Sect. B Struct. Sci.*, 2002, **58**, 380–388.

41 C. F. Macrae, P. R. Edgington, P. McCabe, E. Pidcock, G. P. Shields, R. Taylor, M. Towler and J. van de Streek, *J. Appl. Crystallogr.*, 2006, **39**, 453–457.

42 A. L. Spek, *J. Appl. Crystallogr.*, 2003, **36**, 7–13.

43 Louis J. Farrugia, *J. Appl. Crystallogr.*, 2012, **45**, 849–854.

44 S. K. Wolff, D. J. Grimwood, J. J. McKinnon, D. Jayatilaka and M. A. Spackman, 2017.

45 United States Pharmacopeia and National Formulary USP 29-NF 24, 2006.

46 A. P. Ayala, H. W. Siesler and S. L. Cuffini, *J. Raman Spectrosc.*, 2008, **39**, 1150–1157.

47 M. Karashima, K. Kimoto, T. Kojima and Y. Ikeda, *J. Cryst. Growth*, 2014, **390**, 30–37.

48 G. Gilli, F. Bellucci, V. Ferretti and V. Bertolasi, *J. Am. Chem. Soc.*, 1989, **111**, 1023-1028.

49 L. W. Dittert and T. Higuchi, *J. Pharm. Sci.*, 1963, **52**, 852–857.

50 F. P. Norberto, S. P. Santos, J. Iley, D. B. Silva and M. Corte Real, *J. Braz. Chem. Soc.*, 2007, DOI: 10.1590/S0103-50532007000100019